The Journal of Immunology

Lymphocyte Electrotaxis In Vitro and In Vivo

Francis Lin, Fabio Baldessari, Christina Crenguta Gyenge, Tohru Sato, Robert D. Chambers, Juan G. Santiago and Eugene C. Butcher

J Immunol 2008; 181:2465-2471; ;
doi: 10.4049/jimmunol.181.4.2465
http://www.jimmunol.org/content/181/4/2465

The Journal of Immunology is published twice each month by
The American Association of Immunologists, Inc.,
1451 Rockville Pike, Suite 650, Rockville, MD 20852

Print ISSN: 0022-1767 Online ISSN: 1550-6606.

Lymphocyte Electrotaxis In Vitro and In Vivo[1]

Francis Lin,[2,3]*‡ Fabio Baldessari,[2†] Christina Crenguta Gyenge,*‡ Tohru Sato,*‡ Robert D. Chambers,† Juan G. Santiago,† and Eugene C. Butcher[3]*‡

Electric fields are generated in vivo in a variety of physiologic and pathologic settings, including penetrating injury to epithelial barriers. An applied electric field with strength within the physiologic range can induce directional cell migration (i.e., electrotaxis) of epithelial cells, endothelial cells, fibroblasts, and neutrophils suggesting a potential role in cell positioning during wound healing. In the present study, we investigated the ability of lymphocytes to respond to applied direct current (DC) electric fields. Using a modified Transwell assay and a simple microfluidic device, we show that human PBLs migrate toward the cathode in physiologically relevant DC electric fields. Additionally, electrical stimulation activates intracellular kinase signaling pathways shared with chemotactic stimuli. Finally, video microscopic tracing of GFP-tagged immunocytes in the skin of mouse ears reveals that motile cutaneous T cells actively migrate toward the cathode of an applied DC electric field. Lymphocyte positioning within tissues can thus be manipulated by externally applied electric fields, and may be influenced by endogenous electrical potential gradients as well. ***The Journal of Immunology,*** **2008, 181: 2465–2471.**

Directed cell migration is essential to numerous physiological processes including immune responses, wound healing, cancer metastasis, and neuron guidance (1–3). Chemotaxis and haptotaxis, directed migration in response to soluble or surface bound chemoattractant gradients, have been well characterized. In addition to chemical signals, an electric field can be generated in vitro and in vivo, and such fields can also direct cell movement in a process called electrotaxis or galvanotaxis (4–6). In vitro studies have demonstrated electrotaxis of a number of different cell types in response to direct current (DC)[4] electric fields of a magnitude experienced in vivo (e.g., in healing wounds) (4–6). Some cells migrate toward the cathode (e.g., neural crest cells, fibroblasts, keratinocytes, rat prostate cancer cells, mouse neutrophils, human myeloid cell lines, and many epithelial cell types) (7–16), and other cells migrate to the anode (e.g., corneal endothelial cells, and human vascular endothelial cells) (17–19). Such electrotactic mechanisms have the potential to contribute to cellular positioning in multiple physiologic settings (4–6). As one example, disruption of epithelial integrity leads to an electric field oriented toward the wound (0.4–1.4 V/cm); surrounding epithelial cells migrate directionally to cover the wounded tissue in a process that can be disrupted by interfering with the electric fields (4, 16).

In this study, we have investigated the effects of applied electric fields on the migration of human PBLs. We evaluated T cell responses to electric fields by direct monitoring of migration both in vitro in a controlled chamber environment, and in vivo in mouse skin. Our results show that all circulating lymphocyte classes display electrotaxis to applied electric fields, that the electrotaxis of T cells can be at least as directionally efficient as reported chemotactic responses, and that electric fields can control T cell movement in vivo.

Materials and Methods

Cell preparation

Human buffy coats were obtained from healthy blood donors (The Stanford Blood Center, Stanford, CA). Human PBMC were isolated from the buffy coat using standard gradient centrifugation. Memory T cells ($CD45RA^-CD45RO^+$ T cells) from human PBMC were negatively selected by MACS (magnetic cell separation; Miltenyi Biotec). Human PBMC and purified memory T cells were resuspended in supplemented culture medium (RPMI 1640 GlutaMax medium with 25 mM HEPES buffer (Life Technologies), 1% penicillin-streptomycin and 10% heat-inactivated FBS). The cells were kept in a 37°C incubator with 8% CO_2 injection and were used for experiment within 48 h after separation.

Transwell assay

Cell migration in an applied electric field was tested using Transwell assays (Costar 24-well plate with inserts, 5-μm pore). Briefly, migration medium, consisting of RPMI 1640 with 10% FBS and 10^6 human PBMC in a 100-μl volume, was added to the top well and medium alone was added to the bottom well in a 600-μl volume. An electric field was applied to the Transwell (2.5 V across the Transwell) by placing two platinum electrodes, which were connected to a DC power supply, to the top and bottom well of the Transwell (see Fig. 1*A*). The electrical potential in the Transwell assay was simulated using COMSOL Multiphysics 3.3a (see Fig. 1) (20). The current was measured to be stable for at least 1.5 h. Cells were allowed to migrate from the top well to the bottom well through the filter. The migration of cells in DC electric field was assayed for 1.5 h in a 37°C incubator. Then, the inserts were removed, and the cells that had migrated through the filter to the bottom well were transferred to a FACS tube for staining of different cell markers. Abs against human CD3 (BD Biosciences), CD4 (BD Biosciences), CD8 (eBioscience), CD45RA (BD Biosciences), CD45RO (BioLegend), CD19 (BD Biosciences), and CD56 (BD Biosciences) were used following the manufacturer's recommendation. The stained cell samples were mixed with calibration beads (10,000 beads in 50 μl; Polysciences) and were analyzed using a flow cytometer (LSR-II

*Laboratory of Immunology and Vascular Biology, Department of Pathology, School of Medicine, and †Department of Mechanical Engineering, Stanford University, Stanford, CA 94305; and ‡Center for Molecular Biology and Medicine, Veterans Affairs Palo Alto Health Care System, Palo Alto, CA 94304

Received for publication October 24, 2007. Accepted for publication June 2, 2008.

The costs of publication of this article were defrayed in part by the payment of page charges. This article must therefore be hereby marked *advertisement* in accordance with 18 U.S.C. Section 1734 solely to indicate this fact.

[1] This work is supported by Postdoctoral Training Grant 5T32AI07290-20 from the National Institute of Allergy and Infectious Diseases, National Institutes of Health, to the Immunology Program, Stanford University and a grant from the Stanford Bio-X Interdisciplinary Initiative Program (to F.L.). F.B., E.C.B., and J.G.S. are also supported by a grant from the Stanford Bio-X Interdisciplinary Initiative Program. This work is also supported by Grant R03DK069395 from the National Institutes of Health (to T.S.). This study is supported in part by grants from the National Institutes of Health (to E.C.B. and J.G.S.), and an award from the Department of Veterans Affairs (to E.C.B.).

[2] F.L. and F.B. contributed equally to this work.

[3] Address correspondence and reprint requests to Dr. Francis Lin and Dr. Eugene C. Butcher, Laboratory of Immunology and Vascular Biology, Department of Pathology, School of Medicine, Stanford University, Stanford, CA 94305. E-mail addresses: flin2@stanford.edu and ebutcher@stanford.edu

[4] Abbreviations used in this paper: DC, direct current; EI, electrotactic index.

systems; BD Biosciences). The FACS data were further analyzed using FlowJo (Tree Star). The percentage of migrated cells of each cell type was calculated. The same experiment was repeated with reversed DC electric field or without the field for comparison. Each experimental condition was repeated multiple times ($n = 9–11$). The average and the SEM were calculated for each condition, and the Student t test was performed for comparison ($p < 0.05$). Note that the range of potentials that can be evaluated in this system is limited: current values observably fluctuated at lower fields (presumably due to operating near the subohmic regime). Higher fields were difficult in our setup due to the generation of electrolysis bubbles.

Preparation of microfluidic device

The microfluidic device was fabricated in optically clear plastic, which contains laser-cut microchannels (see Fig. 3). Briefly, each microfluidic device consists of a microscope glass slide (75 mm × 25 mm × 1 mm; VWR), one 100-μm thick Melinex sheet with adhesive on both sides (Fralock Division-Lockwood Industries), one 50-μm thick Melinex sheet with no adhesive (Fralock Division-Lockwood Industries), and two 200-μl pipette tips. The glass slide constitutes the bottom of the microfluidic device. The 100-μm thick Melinex sheet constitutes the sidewalls of the microchannel. For rapid prototyping, we used a CO_2 laser cutter (Universal Laser Systems) to machine the intended channel shape in this sheet. Each channel was ~1.5 cm in length, 500 μm in width, and 100 μm in depth. For the wells, we cut 1.5-mm diameter holes at both ends of the channel. Similarly, we cut 1.5-mm diameter holes in the 50-μm thick Melinex sheet. The 50-μm thick sheet was used to seal the top of the channel, and the holes were cut in correspondence to the wells of the channel. We designed the channel layout using the software AutoCAD (AutoDESK). For assembly, the double-adhesive Melinex sheet was potted onto the precleaned glass slide. The microchannel was sealed using the 50-μm thick sheet, aligning the holes with the channel wells. Finally, two 200-μl pipette tips were cut to remove the sharp tips and were each aligned with one hole, and potted with epoxy (Devcon) to serve as medium reservoirs. Before use, the channel was coated with fibronectin (Fisher) for 2 h at room temperature, providing a substrate for cell adhesion and migration. A new device was used for each experiment.

Cell migration experiment in microfluidic device

For each experiment, a few thousand cells were loaded into the microfluidic device from the wells and allowed to settle in the fibronectin-coated channel for ~10 min in a 37°C incubator. Then, ~150 μl of medium (RPMI 1640 with 10% FBS) were added to each reservoir. Two platinum electrodes (0.25 mm in diameter; Omega) connecting to a DC power supply (Agilent Technologies) were placed in the medium reservoirs to complete the circuit. The device was placed on a microscope stage (Axiovert 35; Carl Zeiss) and the system was allowed to equilibrate for ~5 min (wait until no flowing cells were seen in the channel). Then, the DC electric field was applied, and cell migration (in a selected ~550 μm width × 800 μm length microscope field using a 10X objective) was recorded by time-lapse microscopy at 6 frames/min for 30 min to 2 h at room temperature using a solid-state camera (model no. 4815-2000; Cohu). The image acquisition was controlled by VCE Pro (First Vision).

Cell tracking and data analysis

Movement of individual cells was tracked using NIH ImageJ (v.1.34s) (21). Background of the images was subtracted and the noise was removed using the "despeckle" function. Then the images were calibrated to distance. Only the cells that migrated within the microscope field were selected and tracked using the "Manual Tracking" plug-in in NIH ImageJ. The tracking data were exported to Excel and Oriana for analysis. Over 100 cell tracks from multiple independent experiments were analyzed.

The movement of cells was quantitatively evaluated by 1) the percentage of cells that migrated toward the cathode of the electric field; 2) electrotactic index (EI), which is the ratio of the displacement of cells toward the cathode of the electric field (Δy) to the total migration distance (d) using the equation $EI = \Delta y/d$ presented as the average value ± SEM; 3) the average speed (V) calculated as $d/\Delta t$ and presented as the average value ± SEM of all cells; and 4) statistical analysis of migration angles performed using Oriana for Windows (Kovach Computing Services) to examine the directionality of the cell movement. Specifically, migration angles (calculated from x-y coordinates at the beginning and the end of the cell tracks) were summarized in a direction plot, which is a rose diagram showing the distribution of angles grouped in 20-degree intervals, with the radius of each wedge indicating cell number. The Rayleigh test for circular uniformity was applied, with a significance level of 0.05. When there was significant directionality, the mean angle and the 95% confidence interval were calculated. A modified Rayleigh test (V test) was also applied, to test whether deviations from the direction of electric field (90 or 270 degrees) were significant.

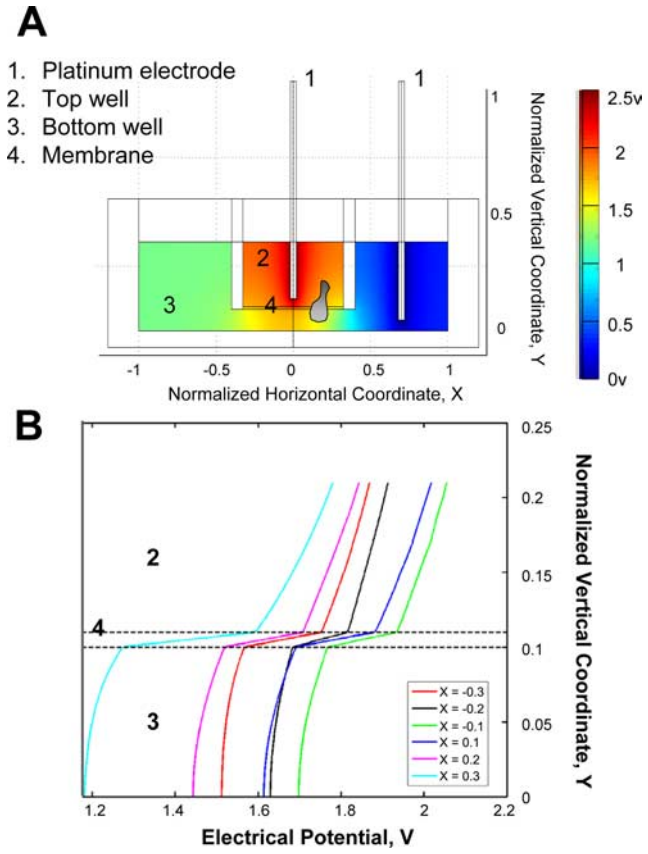

FIGURE 1. Transwell-based electrotaxis assay. *A*, Transwell assay is illustrated for studying cell migration in an applied electric field. An electric field was applied across the Transwell (2.5 V) by placing two platinum electrodes, which were connected to a DC power supply, to the top and bottom well of the Transwell, respectively. Cells were allowed to migrate from the top well to the bottom well through the membrane. The electrical potential in the Transwell assay was simulated. *B*, The simulated electrical potential was plotted as a function of normalized vertical y coordinate for different normalized horizontal x coordinate within the membrane (−0.3–0.3). Normalized x coordinate (1 = 7.8 mm) and y coordinate (1 = 10 mm) are shown.

Phosphorylated flow cytometry

Human PBLs (3.5×10^6) resuspended in 500 μl of RPMI 1640 medium were stimulated in a 24-well plate by an applied electric field (2.5 V across ~1.3 cm for 60 min at room temperature); two platinum electrodes connecting to a DC power supply were placed in the cell-containing medium to generate the electric field. Stimulated cells were immediately fixed in 2% paraformaldehyde in PBS for 10 min at room temperature and then permeabilized in 100% methanol at −20°C overnight. Control cells were treated similarly but without exposure to the electric field. Cells were then washed twice with staining buffer (0.5% BSA in PBS) and stained with Alexa Fluor 488-conjugated phospho-Erk1/2 (T202/Y204) or Alexa Fluor 647-conjugated phospho-Akt-Ser^{473} Ab (BD Biosciences). Cells were analyzed using a flow cytometer (LSR-II systems; BD Biosciences). The FACS data were further analyzed using FlowJo (Tree Star).

Confocal microscopy of cell migration in mouse ear tissue

Transgenic mice heterozygous for *Cxcr6* (*Cxcr6gfp/+*), B6.129P2-*Cxcr6tm1Litt*/J crossed with C57BL/6J (The Jackson Laboratory) were used. These mice have one *Cxcr6* allele replaced by enhanced GFP marking activated and memory CD4 and CD8 T cells fluorescent green, which can be visualized by fluorescent microscopy and flow cytometry (22). The in vivo imaging experiments were performed under an approved animal use protocol. For each experiment, a *Cxcr6gfp/+* mouse was anesthetized

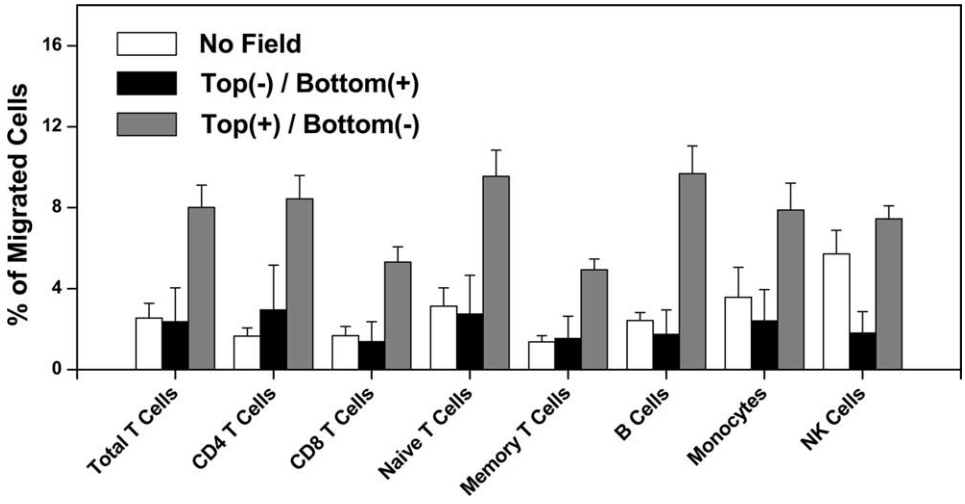

FIGURE 2. Migration of human PBLs and monocytes in an applied electric field. The rate of migration of different subsets of human PBMC increased in Transwell assay when the electric field was configured with the positive electrode in the top well and the negative electrode in the bottom well (Top(+)/Bottom(−)) compared with migration in the reversed electric field (Top(−)/Bottom(+)) or without the field. Error bars represent the SEM of multiple independent experiments (n = 9–11).

by inhaled isoflurane (Table Top Lab Animal Anesthesia System; VetEquip) followed by ketamine/xylazine anesthesia. Under anesthesia, two platinum electrodes (0.25 mm in diameter; Omega) connecting to a DC power supply (Agilent Technologies) were surgically inserted to the peripheral tissue of the mouse ear, ~5 mm apart. Then the mouse was placed on the stage of a confocal microscope (LSM 510 META; Carl Zeiss), and the ear was pressed onto a glass coverslide, which was mounted on the slide holder. The rest of the mouse body was electrically isolated from the microscope stage. The GFP-positive cells in the mouse ear was imaged (argon laser, 488 nm wavelength) with or without the externally applied DC electric field (1–2.5 V across ~5 mm) for 1–2 h at ~80 s per scanning cycle using a 10X or a 20X objective. For each scanning cycle, 20 images at 5-μm intervals along the z direction were captured. The "stack" of images associated with each scanning cycle was then depth-averaged and processed in MATLAB (MathWorks). Using the DIPimage MATLAB package (Quantitative Imaging Group Delft, NL), we aligned, background-subtracted, and conditioned each frame to remove stationary features. We then tracked the moving cells with a particle tracking velocimetry algorithm (D. Blair and E. Dufresne, http://physics.georgetown.edu/matlab/). Briefly, the algorithm located cells' centroids with subpixel accuracy and tracked cells between frames using a χ^2 minimization process based on cell displacement, constrained by a maximum cell velocity. To reduce noise, we ignored cells that were tracked for fewer than five frames or that were not sufficiently displaced (less than 2 cell diameters). We chose threshold parameters, which maximized the number of tracked cells without causing discernible false positives. The tracking data were further analyzed to calculate the displacement of each cell in the x and y direction, and the EI.

Results

Electrotactic response of human PBLs and peripheral blood monocytes in Transwell assays

We applied the Transwell assay, a conventional method for studies of leukocyte chemotaxis, to determine whether PBMCs would respond to an applied electric field. Platinum electrodes were arranged in the top and bottom wells to allow application of an electric field (see *Materials and Methods*) (Fig. 1*A*). Numerical simulations using specialized modeling software COMSOL Multiphysics 3.3a were used to model the configuration: the simulation indicates that application of 2.5 V across the Transwell yields an electrical potential gradient along the vertical direction in the top well that is close to the physiologic range seen in wounds (Fig. 1). Human PBMC were added to the top well and allowed to migrate in the presence or absence of the applied field. Immunofluorescence staining and cytometric analysis of input and migrated cell populations allowed assessment of the efficiency of migration of each of the human PBMC subsets indicated (Fig. 2).

Compared with spontaneous migration in the absence of a field, there was a significant increase in migration of all lymphocyte subsets except NK cells when the cathode was in the bottom well. Moreover, the magnitude of the effect was similar for CD4 T cells, CD8 T cells, naive T cells, memory T cells, B cells, and for monocytes. In contrast, migration was not enhanced when the field was applied in the opposite orientation, indicating that the migration is directional. Compared with other blood lymphocytes, NK cells displayed high background migration (a well-known characteristic of these cells), potentially obscuring any electrotaxis. Moreover, when the field was reversed NK cell migration to the bottom well was suppressed below background, supporting an electrotactic response to the cathode in the top well (Fig. 2). Thus, these results support the hypothesis that human PBLs and monocytes undergo cathode-directed electrotaxis, and that in contrast to chemotactic

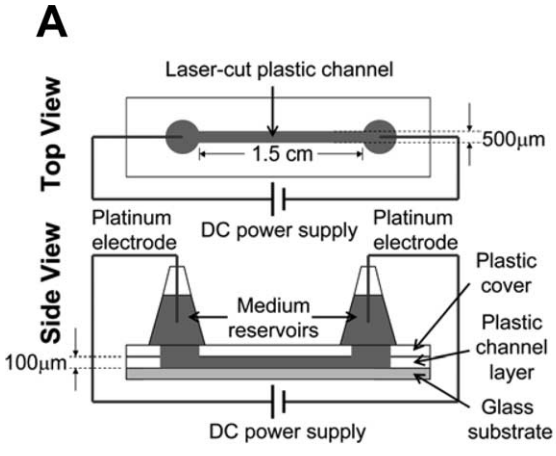

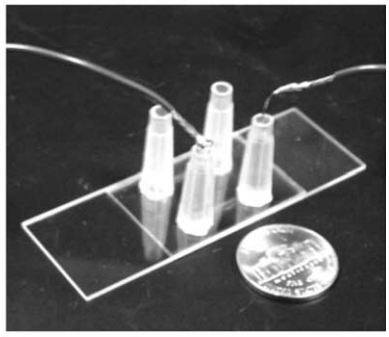

FIGURE 3. Microfluidic chamber for visualization of cell migration in an applied electric field. *A*, Microfluidic system is illustrated for studying cell migration in an applied electric field. *B*, An image of the microfluidic system. Two identical channels were configured side-by-side in a single device and can be used for migration studies separately. A nickel was placed next to the device as a scale reference.

receptor-driven responses, which are characteristically subset-selective, the electrotactic response is remarkably uniform among the major lymphocyte classes.

Electrotaxis of memory T cells in a microfluidic visualization chamber

To confirm and visualize the lymphocyte electrotactic response and evaluate the efficiency of orientation of migrating cells toward the cathode in controlled electric fields, we traced the migration of purified memory T cells from human PBMC migrating on a fibronectin-coated coverslide (see *Materials and Methods*) (Fig. 3). A synthesized channel and medium reservoirs were filled with migration medium, cells were added and allowed to adhere, and the electric field was applied using platinum electrodes in the two medium reservoirs. The migratory behavior of cells in the channel was recorded by video microscopy. Compared with the Transwell assay, the microfluidic device can generate a well-defined uniform electric field in the microchannel, and allows visualization and quantitative assessment of cell migration.

We applied an electric field of 1 V/cm, similar to fields observed in wound tissue (16). The field induced a current on the order of 2 μA, which was stable over the 1.5-h period. Almost all adherent T cells migrated, and a high percentage migrated toward the cathode of the applied electric field (Fig. 4*C*). The EI (mathematically analogous to the widely used chemotactic index (21, 23–25)) is presented (Fig. 4*C*). Statistical analysis of migration angles shows that the distribution of migration angles is highly correlated with the direction of the applied electric field (Fig. 4*B*). The quantitative analysis also agrees with direct visualization of cell tracks (Fig. 4*A*). In addition, the cells exhibited a relatively high migration speed in the electric field (Fig. 4*C*), comparable to the optimal speed of T cells we observed in response to chemoattractant stimuli (21). No significant movement of cells was detected in the absence of an applied electric field: cells in this model are adherent and nonmotile in the absence of a chemoattractant or electric field (data not shown). When the electric field was inverted, the cells reversed direction and now migrated toward the new cathode (Fig. 4, *D–F*). We conclude that T cell migration can be directed by physiologically relevant applied electric fields in vitro. The efficiency of migration (the EI) is slightly higher than the chemotactic index we observed in a similar study tracing T cell chemotaxis (21), and higher than the optimal chemotactic index we observed in earlier studies of neutrophil chemotaxis in agarose assays (26, 27) and a three-dimensional fibrin gel assay (25).

Electric fields induce T cell signaling responses

Directional migration of cells is orchestrated by a cascade of intracellular signaling events that coordinate actin polymerization, membrane and cellular polarization, protrusion, and adhesion mechanisms (28). Well-characterized intracellular responses to chemoattractants include activation of kinase cascades such as phosphorylation of Erk1/2 (a member of MAPK family) (29) and Akt (a downstream signaling molecule of PI3K pathway). Kinase responses have also been associated with electrotaxis of neutrophils (16). To confirm triggering of intracellular signals in lymphocytes, we applied an electric field and measured its effects on Erk1/2 and Akt in human PBLs using flow cytometric methods (see *Materials and Methods*).

As shown in Fig. 5, Erk1/2 and Akt phosphorylation were increased in cells exposed for 60 min to an electric field, confirming the engagement of intracellular kinase cascades. Shorter electrical stimulation (i.e., 1 or 10 min) did not induce detectable increases of Erk1/2 or Akt phosphorylation (data not shown). Thus, intra-

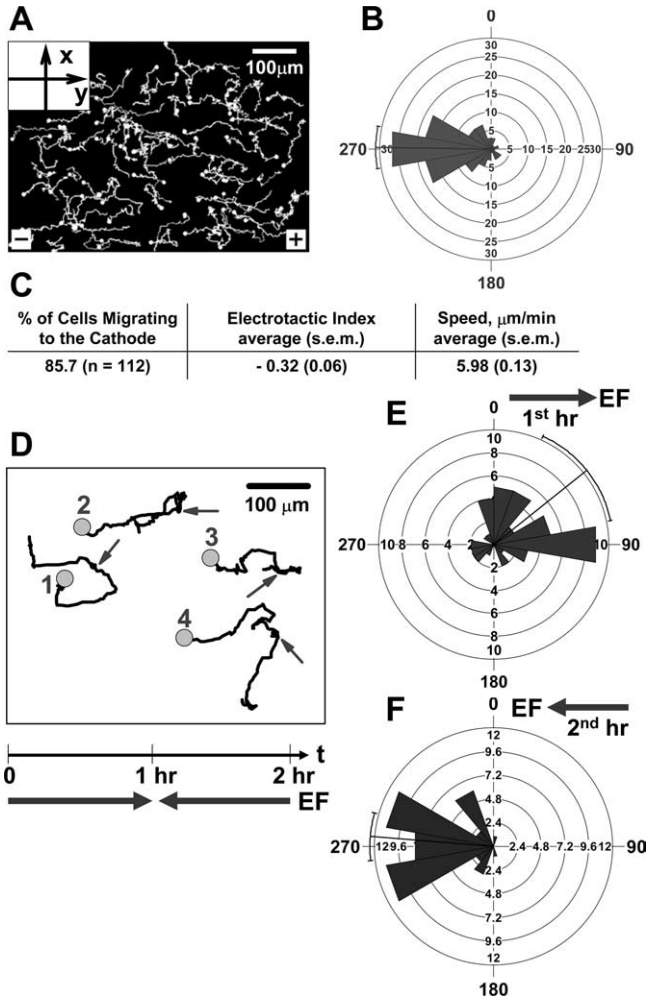

FIGURE 4. Directional migration of memory T cells in an applied electric field in vitro. *A*, Cell tracks of a representative experiment show that cells preferentially migrate toward the cathode to the left of the electric field (angle 270 degree). An electric field (1 V/cm) was applied and the migration of cells was recorded for 30 min at 6 frames/min. The solid circles indicate the end of the tracks. *B*, The rose diagram shows the distribution of migration angles (the migration angles were calculated from *x-y* coordinates at the beginning and end of the cell tracks, and were grouped in 20-degree intervals, with the radius of each wedge indicating the cell number). Mean angle vector and the 95% confidence interval were also shown. Rayleigh uniformity test confirmed that the distribution of migration angles is not uniform. The Modified Rayleigh test (V test) showed that the deviation of the migration angles from the direction of electric field (270 degree) is not significant. *C*, The percentage of cells migrated toward the cathode of the electric field. EI and the speed data that were calculated using over 100 cell tracks from at least three independent experiments are presented. EI and speed are presented as the average value ± SEM of all cells. *D–F*, Effects of field reversal. *D*, Four representative cell tracks showing that cells migrated toward the cathode of the electric field and followed the reverse of the electric field (90 to 270 degrees at the 60th min). An electric field to the right (1 V/cm) was applied for 1 h and was reversed (to the left) for another hour. Migration of cells was recorded continuously for 2 h at 6 frames/min. Circles indicate the end of the tracks and the arrows indicate when the electric field was reversed. Rose diagrams show the distribution of migration angles in the first hour (*E*) and the second hour (*F*) of the experiment (the migration angles were calculated from *x-y* coordinates at the beginning and the end of the cell tracks ($n = 45$), and were grouped in 20-degree intervals, with the radius of each wedge indicating cell number. The mean angle vector and the 95% confidence interval were also shown. Rayleigh uniformity test confirmed that the distribution of migration angles is not uniform. The Modified Rayleigh test (V test) showed that the deviations of the migration angles from the direction of electric field (90 degrees in the first hour and 270 degrees in the second hour) are not significant.

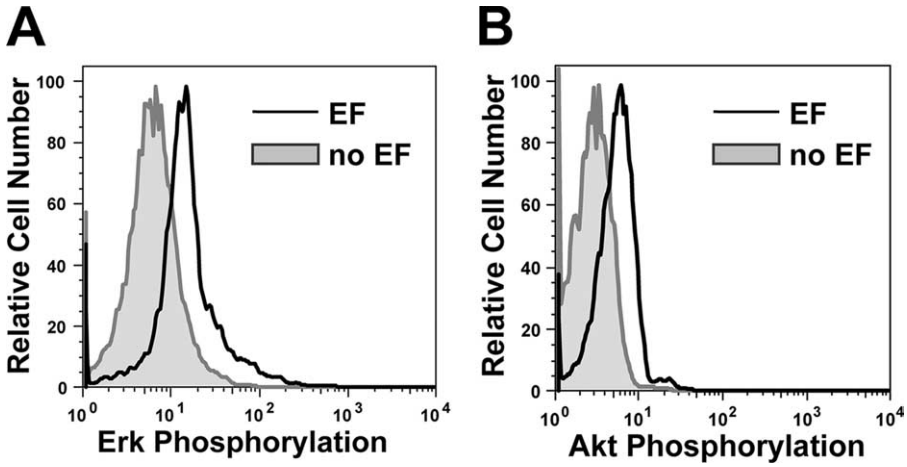

FIGURE 5. Signaling of human PBLs in an applied electric field. Phosphorylation of Erk1/2 (*A*) and Akt (*B*) is increased in an applied electric field as measured by phosphorylated flow cytometry. Cells were stimulated by an electric field (2.5 V across ~1.3 cm) for 60 min at room temperature in a 24-well plate. Stimulated cells, and unstimulated control cells incubated in parallel but without an electric field, were stained with anti-phospho-Erk1/2 Ab or anti-phospho-Akt-Ser^{473} Ab. Each experiment was repeated at least three times with similar results.

cellular signaling events shared with chemotactic responses are triggered in lymphocytes activated by an electric field.

T cell electrotaxis in vivo

As mentioned, epithelial injury induces an electric field oriented toward the wound and similar in magnitude to that used in our experiments (16), suggesting a potential role for electrotaxis in recruitment of regulatory or memory T cells and other leukocytes from surrounding tissue. Analyzing leukocyte electrotaxis in response to physiologic electric field produced by a wound, however, is complicated by the fact that tissue injury releases multiple chemoattractants, to which subsets of T cells also respond. We therefore asked whether an externally applied electric field can direct migration of lymphocytes in vivo in a homeostatic setting, in which inflammatory chemotactic mechanisms can be distinguished from electric field-induced cellular responses. We took advantage of genetically modified mice which express GFP under the promoter of the chemokine receptor CXCR6 (30). In these mice, GFP is highly expressed in subsets of tissue lymphocytes, allowing their movement to be followed by time-lapse confocal microscopy. Imaging in the living ear reveals scattered small GFP-positive cells, with morphological characteristics consistent with polarized migrating lymphocytes (Fig. 6*A*, circled cells). Most of these small GFP-positive cells were spontaneously motile (Fig. 6*B*). Consistent with expression of CXCR6 by γδ T cells (31), flow cytometric analysis reveals that among cells rendered efficiently into suspension (a process that enriches lymphocytes), most lymphocytic cells isolated from ear skin are CD3$^+$ (76% of GFP-positive cells), and many express γδ TCR (56% of total GFP-positive cells). A more abundant GFP-positive population, consisting of larger cells with dendritic morphology, is also present in the ear skin; these cells are prominent in confocal fluorescence imaging (Fig. 6*A*, cells not circled) and were sessile over the periods of observation studied, whether or not an external electric field was applied.

In the absence of an applied electric field (with electrodes inserted into the ear but without voltage), the lymphocytic GFP cells migrated randomly (Fig. 6*B* and supplemental video 1).[5] When an electric field was applied (1–2.5 V across ~5 mm in the peripheral

[5] The online version of this article contains supplemental material.

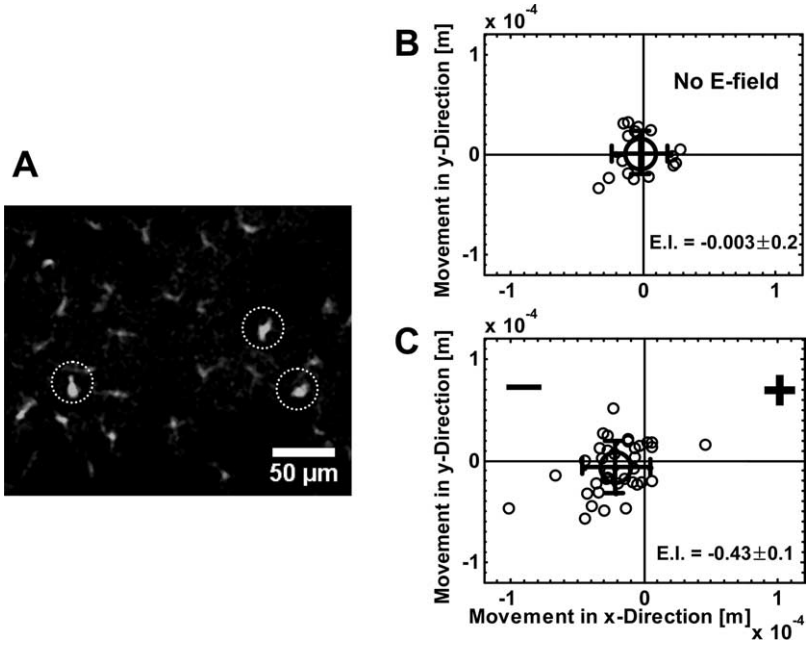

FIGURE 6. Migration of T cells in mouse ear pinna in response to an applied electric field. *A*, Confocal image of CXCR6$^+$ (GFP-positive) cells in the ear tissue of a CXCR6 GFP transgenic mouse. image selected from a single focal plane. The cells in circles are the migrating cells. These cells with lymphocytic morphology are motile and are typically outnumbered by sessile GFP-positive cells of dendritic morphology in the ear tissue as visualized by confocal microscopy. *B*, Distribution of motile lymphocytic cell displacement along the *x* and *y* direction in the absence of an applied electric field. The large circle is the average cell displacement. Error bar represents SD. *C*, Distribution of motile lymphocytic cell displacement along the *x* and *y* direction in an applied electric field (2.5 V across ~5 mm in the ear tissue). The large circle is the average cell displacement. Error bar represents SD. Note that most cells were within the visible focal plane for only a fraction of the 1–2 h visualization period. The EI is also shown as the average ± SEM.

ear tissue), however, these GFP cells preferentially migrated toward the cathode within the microscope field. The negative electrode was located ~2 mm from the microscope field. Individual cells migrated as much as 100 μm toward the cathode over the 1–2 h period of experiment (Fig. 6*C* and supplemental video 2). It is worth pointing out that the images were depth averaged and projected onto a common two-dimensional plane for tracking analysis. However, some cells moved outside of the visible field in the z direction and were lost from analysis during the observation period. Therefore the mean distance of cell migration visualized was less than the actual migration distance in three-dimensional tissues. The velocity of migration of motile cells was similar in the presence or absence of the applied field (i.e., 0.34 ± 0.02 μm/min (average ± SEM) in the absence of the field vs 0.43 ± 0.04 μm/min (average ± SEM) in the applied field, $p=0.17$). We conclude that lymphocytes can be directed in vivo by externally applied electric fields.

Discussion

Our studies show that normal blood lymphocytes and monocytes respond to a steady electric field in Transwell assays. All lymphocyte subsets examined, including naive and memory CD4, CD8 T cells, and B cells migrated toward the cathode, as did monocytes. Electrotactic migration is highly directional: that in studies monitoring the migratory path of memory T cells on fibronectin-coated glass, almost all cells migrated cathodally, and the directionality index is comparable to or higher than the optimal directionality index observed in comparable chemotaxis assays. We also confirm that electric field exposure induces Erk1/2 and Akt activation in lymphocytes, consistent with activation of the MAPK and PI3K signaling pathways implicated in coordinated cell motility. Finally, we show that an applied electric field induced the electrotactic migration of endogenous lymphocytes in mouse skin. Our results thus define electrotaxis as potentially an additional mechanism for the control of lymphocyte and monocyte migration.

Electrotaxis of eukaryotic cells has been reported in a number of studies (4, 6). Particularly, electrotaxis of epithelial cells plays an important role in controlling wound healing (i.e., the wound generates an inward DC electric field and electrotaxis of epithelial cells toward the cathode of the electric field helps closing the wound) (4, 16). Our results show that memory T cells migrate toward the cathode of an electric field applied with strength similar to wound generated electric field. Therefore, electrotaxis of lymphocytes and other immune cells may be involved in the process of wound healing as well. Furthermore, our study shows that immune cell positioning can be regulated in vivo by externally applied electric fields.

An interesting aspect of our results is the uniformity in the electrotactic responses of different mononuclear leukocyte subsets as assessed in the Transwell assay. This response contrasts with responses to known chemoattractants for which cell surface receptors are differentially expressed and direct subset-selective migration. The uniform migration of circulating lymphocytes suggests that other leukocyte subsets (e.g., tissue memory cells) may undergo electrotaxis as well. In contrast, not all GFP-positive cells in mouse skin responded: rather the electrotactic responses appeared limited to cells that were intrinsically motile, i.e., cells that displayed random migration before field application. Thus, leukocyte responses to electric potential gradients may be regulated primarily by the migratory state of competence of the cells, rather than (as in the case of chemotactic response) by subset specificity among migratory populations.

Indeed, as suggested by the diverse cell types that respond, from *Dictyostelium amoebae* to epithelial cells, metastatic cancer cells, and lymphocytes, electrotaxis may be a nearly universal competency of motile cells (4, 6). Regulation of electrotaxis may be possible in terms of directionality, however. Although lymphocytes, like many other mammalian cells, undergo cathode-directed electrotaxis, some cells (e.g., corneal endothelial cells, human vascular endothelial cells) migrate preferentially to the anode. Given the absence of subset selectivity in lymphocyte responses, however, it seems unlikely that electric fields operate in vivo to control the recruitment of lymphocytes from the blood or direct their microenvironmental interactions during physiologic immune responses. Instead, physiologic electric fields may serve to support cellular translocation events in settings in which cell type specificity is not a critical issue. One example would be the bulk cell population movements that occur early in embryogenesis, when the principal distinction is between motile and nonmotile undifferentiated cells; indeed the role of electric fields in cell movement was implicated in studies of early embryogenesis (4, 5). A more pertinent example is the cellular response to a penetrating wound, during which the rapid recruitment of any motile cell (fibroblasts, macrophages and other immune cells) from the immediately surrounding tissue would seem beneficial or at least not deleterious. As mentioned at the start of this report, epithelial surfaces such as the skin are well-documented batteries, maintaining an electrical potential gradient that is short circuited upon disruption of the epithelial barrier. Wounds in bovine cornea or in guinea pig and human skin, for example, generate local electric fields of 0.4–1.4 V/cm with the wound itself being the cathode. This field is well within the range for efficient electrotactic recruitment of lymphocytes and other motile cells into the wound. Although in the case of lymphocytes and other immune cells it may be difficult in such a setting to isolate the effects of electrotaxis from those of the chemoattractants induced, our studies clearly show that lymphocytic cells resident in skin respond with directional migration when presented with an applied electric field.

Previous studies have found that electric fields activate intracellular signaling processes including kinase pathways involved in cellular motility. We have confirmed in this study that lymphocytes respond to electric fields with activation of Erk kinases and Akt, which are involved in chemoattractant receptor signaling and in electrotactic signaling in other cells (16, 29, 32). Activation of these pathways suggests that electrotaxis and chemotaxis engage common intracellular cell motility programs in responding lymphocytes. In contrast, in keeping with findings in *Dictyostelium amoebae* in which electric fields did not generate a rapid burst of calcium signaling (but only a slow, prolonged calcium response) at the population level (32), we did not observe a robust, immediate calcium flux in lymphocytes in response to electrical stimulation, and delayed calcium elevation assessed by flow cytometric analysis of Fluo-4 labeled cells was variable (data not shown). The kinetics of MAPK and Akt signaling also distinguishes the electric field response because phosphorylation of Erk and Akt was significant after 60 min, but was not appreciable by phospho-flow analyses at 1 or 10 min, contrasting with the rapid triggering of signaling cascades by chemoattractant receptors.

In conclusion, our study demonstrates electrotaxis of lymphocytes, and shows that electric fields can direct lymphocyte migration in vitro and in vivo. Electrotaxis represents an additional mechanism for the control of leukocyte migration. It is likely to play a role in sites of epithelial injury, and may permit novel approaches for manipulating the positioning of lymphocytes and other immunocytes to enhance vaccine or antitumor responses.

Acknowledgments

We thank The Stanford Blood Center for technical support. We thank Tarun Khurana for helping with the fabrication of microfluidic devices, and Dr. Hekla Sigmundsdottir and Lusijah Rott for helping with flow cytometry.

Disclosures

The authors have no financial conflict of interest.

References

1. Condeelis, J., J. Jones, and J. Segall. 1992. Chemotaxis of metastatic tumor cells: clues to mechanisms from the *Dictyostelium* paradigm. *Cancer Metastasis Rev.* 11: 55–68.
2. Kubes, P. 2002. Introduction: The complexities of leukocyte recruitment. *Semin. Immunol.* 14: 65–72.
3. Song, H., and M. Poo. 1999. Signal transduction underlying growth cone guidance by diffusible factors. *Curr. Opin. Neurobiol.* 9: 355–363.
4. McCaig, C. D., A. M. Rajnicek, B. Song, and M. Zhao. 2005. Controlling cell behavior electrically: current views and future potential. *Physiol. Rev.* 85: 943–978.
5. Robinson, K. R., and M. A. Messerli. 2003. Left/right, up/down: the role of endogenous electrical fields as directional signals in development, repair and invasion. *BioEssays* 25: 759–766.
6. Mycielska, M. E., and M. B. Djamgoz. 2004. Cellular mechanisms of direct-current electric field effects: galvanotaxis and metastatic disease. *J. Cell Sci.* 117: 1631–1639.
7. Cooper, M. S., and R. E. Keller. 1984. Perpendicular orientation and directional migration of amphibian neural crest cells in DC electrical fields. *Proc. Natl. Acad. Sci. USA* 81: 160–164.
8. Sheridan, D. M., R. R. Isseroff, and R. Nuccitelli. 1996. Imposition of a physiologic DC electric field alters the migratory response of human keratinocytes on extracellular matrix molecules. *J. Invest. Dermatol.* 106: 642–646.
9. Onuma, E. K., and S. W. Hui. 1985. A calcium requirement for electric field-induced cell shape changes and preferential orientation. *Cell Calcium* 6: 281–292.
10. Djamgoz, M. B. A., M. Mycielska, Z. Madeja, S. P. Fraser, and W. Korohoda. 2001. Directional movement of rat prostate cancer cells in direct-current electric field: involvement of voltagegated Na^+ channel activity. *J. Cell Sci.* 114: 2697–2705.
11. Zhao, M., A. Dick, J. V. Forrester, and C. D. McCaig. 1999. Electric field-directed cell motility involves up-regulated expression and asymmetric redistribution of the epidermal growth factor receptors and is enhanced by fibronectin and laminin. *Mol. Biol. Cell* 10: 1259–1276.
12. Zhao, M., C. D. McCaig, A. Agius-Fernandez, J. V. Forrester, and K. Araki-Sasaki. 1997. Human corneal epithelial cells reorient and migrate cathodally in a small applied electric field. *Curr. Eye Res.* 16: 973–984.
13. Zhao, M., A. Agius-Fernandez, J. V. Forrester, and C. D. McCaig. 1996. Directed migration of corneal epithelial sheets in physiological electric fields. *Invest. Ophthalmol. Vis. Sci.* 37: 2548–2558.
14. Zhao, M., A. Agius-Fernandez, J. V. Forrester, and C. D. McCaig. 1996. Orientation and directed migration of cultured corneal epithelial cells in small electric fields are serum dependent. *J. Cell Sci.* 109(Pt. 6): 1405–1414.
15. Li, X., and J. Kolega. 2002. Effects of direct current electric fields on cell migration and actin filament distribution in bovine vascular endothelial cells. *J. Vasc. Res.* 39: 391–404.
16. Zhao, M., B. Song, J. Pu, T. Wada, B. Reid, G. Tai, F. Wang, A. Guo, P. Walczysko, Y. Gu, et al. 2006. Electrical signals control wound healing through phosphatidylinositol-3-OH kinase-γ and PTEN. *Nature* 442: 457–460.
17. Rapp, B., A. de Boisfleury-Chevance, and H. Gruler. 1988. Galvanotaxis of human granulocytes: dose-response curve. *Eur. Biophys. J.* 16: 313–319.
18. Chang, P. C., G. I. Sulik, H. K. Soong, and W. C. Parkinson. 1996. Galvanotropic and galvanotaxic responses of corneal endothelial cells. *J. Formos. Med. Assoc.* 95: 623–627.
19. Zhao, M., H. Bai, E. Wang, J. V. Forrester, and C. D. McCaig. 2004. Electrical stimulation directly induces pre-angiogenic responses in vascular endothelial cells by signaling through VEGF receptors. *J. Cell Sci.* 117: 397–405.
20. Seghir, T., D. Mahi, T. Lebey, and D. Malec. 2006. Analysis of the electric field and the potential distribution in cavities inside solid insulating electrical materials. *Proceedings of the COMSOL Users Conference at Paris, November 7–9*. Multiphysics, Paris, France.
21. Lin, F., and E. C. Butcher. 2006. T cell chemotaxis in a simple microfluidic device. *Lab Chip* 6: 1462–1469.
22. Unutmaz, D., W. Xiang, M. J. Sunshine, J. Campbell, E. Butcher, and D. R. Littman. 2000. The primate lentiviral receptor Bonzo/STRL33 is coordinately regulated with CCR5 and its expression pattern is conserved between human and mouse. *J. Immunol.* 165: 3284–3292.
23. Lin, F., C. Nguyen, S. Wang, W. Saadi, S. Gross, and N. Jeon. 2005. Neutrophil migration in opposing chemoattractant gradients using microfluidic chemotaxis devices. *Ann. Biomed. Eng.* 33: 475–482.
24. Lin, F., C. M. Nguyen, S. J. Wang, W. Saadi, S. P. Gross, and N. L. Jeon. 2004. Effective neutrophil chemotaxis is strongly influenced by mean IL-8 concentration. *Biochem. Biophys. Res. Commun.* 319: 576–581.
25. Moghe, P. V., R. D. Nelson, and R. T. Tranquillo. 1995. Cytokine-stimulated chemotaxis of human neutrophils in a 3-D conjoined fibrin gel assay. *J. Immunol. Methods* 180: 193–211.
26. Foxman, E. F., J. J. Campbell, and E. C. Butcher. 1997. Multistep navigation and the combinatorial control of leukocyte chemotaxis. *J. Cell Biol.* 139: 1349–1360.
27. Foxman, E. F., E. J. Kunkel, and E. C. Butcher. 1999. Integrating conflicting chemotactic signals: the role of memory in leukocyte navigation. *J. Cell Biol.* 147: 577–588.
28. Chung, C. Y., S. Funamoto, and R. A. Firtel. 2001. Signaling pathways controlling cell polarity and chemotaxis. *Trends Biochem. Sci.* 26: 557–566.
29. Sotsios, Y., G. C. Whittaker, J. Westwick, and S. G. Ward. 1999. The CXC chemokine stromal cell-derived factor activates a G_i-coupled phosphoinositide 3-kinase in T lymphocytes. *J. Immunol.* 163: 5954–5963.
30. Geissmann, F., T. O. Cameron, S. Sidobre, N. Manlongat, M. Kronenberg, M. J. Briskin, M. L. Dustin, and D. R. Littman. 2005. Intravascular immune surveillance by $CXCR6^+$ NKT cells patrolling liver sinusoids. *PLoS Biology* 3: e113.
31. Hayday, A., and R. Tigelaar. 2003. Immunoregulation in the tissues by $\gamma\delta$ T cells. *Nat. Rev. Immunol.* 3: 233–242.
32. Shanley, L. J., P. Walczysko, M. Bain, D. J. MacEwan, and M. Zhao. 2006. Influx of extracellular Ca^{2+} is necessary for electrotaxis in *Dictyostelium*. *J. Cell Sci.* 119: 4741–4748.